

Tagging the chemical evolution history of the Large Magellanic Cloud disk ¹

Emilio Lapenna

Dipartimento di Astronomia, Università degli Studi di Bologna, Via Ranzani, 1 - 40127 Bologna, ITALY

emilio.lapenna2@unibo.it

Alessio Mucciarelli

Dipartimento di Astronomia, Università degli Studi di Bologna, Via Ranzani, 1 - 40127 Bologna, ITALY

alessio.mucciarelli2@unibo.it

Livia Origlia

INAF - Osservatorio Astronomico di Bologna, Via Ranzani, 1 - 40127 Bologna, ITALY

livia.origlia@oabo.inaf.it

and

Francesco R. Ferraro

Dipartimento di Astronomia, Università degli Studi di Bologna, Via Ranzani, 1 - 40127 Bologna, ITALY

francesco.ferraro3@unibo.it

ABSTRACT

We have used high-resolution spectra obtained with the multifiber facility FLAMES at the Very Large Telescope of the European Southern Observatory to derive kinematic properties and chemical abundances of Fe, O, Mg and Si for 89 stars in the disk of the Large Magellanic Cloud (LMC). The derived metallicity and $[\alpha/\text{Fe}]$, obtained as the average of O, Mg and Si abundances, allow us to draw a preliminary scheme of the star formation history occurred in this region of the LMC. The derived metallicity distribution shows two main components: one component (comprising $\sim 84\%$ of the sample) is peaked at $[\text{Fe}/\text{H}] = -0.48$

dex and it shows an $[\alpha/\text{Fe}]$ ratio slightly under solar ($[\alpha/\text{Fe}] \sim -0.1$ dex). This population was probably originated by the main star formation event occurred 3–4 Gyr ago (possibly triggered by tidal capture of the Small Magellanic Cloud). The other component (comprising $\sim 16\%$ of the sample) is peaked at $[\text{Fe}/\text{H}] \sim -1$ dex and it shows an $[\alpha/\text{Fe}] \sim 0.2$ dex. This population was probably generated during the long quiescent epoch of star formation in between the first episode and the most recent bursts. Indeed, in our sample we do not find stars with chemical properties similar to the old LMC globular clusters nor to the iron-rich and α -poor stars recently found in the LMC globular cluster NGC 1718 and predicted to be also in the LMC field, thus suggesting that both these components are small ($< 1\%$) in the LMC disk population.

Subject headings: stars: abundances — Magellanic Clouds — techniques: spectroscopic

1. Introduction

Despite several years of studies, the chemical evolution history of the Large Magellanic Cloud (LMC) as well its star formation history (SFH) is still poorly understood. The LMC has experienced a complex SFH due to the interaction occurred both with the Small Magellanic Cloud (SMC) and the Galaxy (Bekki & Chiba 2005). A clear evidence of this quite complex evolution can be recognized in the LMC star cluster system, characterized by a wide range of age and metallicities. The study of these cluster stellar populations reveals the existence of at least three components: the old (~ 13 Gyr, Brocato et al. 1996, Olsen et al. 1998) metal-poor component ($[\text{Fe}/\text{H}] < -1.5$ dex, Olszewski et al. 1991, Grocholski et al. 2006, Mucciarelli et al. 2010) probably formed during the first episode of star formation (SF), the intermediate age component ($\sim 1\text{--}3$ Gyr, Gallart et al. 2003, Ferraro et al. 2004) which is the dominant one, and a young component ($\lesssim 1$ Gyr, Brocato et al. 2003, Mucciarelli et al. 2011) that include the last formed clusters.

The SFH of field stellar populations is less known. Smecker-Hane et al. (2002) found that the dominant stellar population in the central bar was formed between 4–6 Gyr and 1–2 Gyr ago. This result was substantially confirmed by the simulations of Bekki & Chiba

¹Based on observations collected at the ESO-VLT at Cerro Paranal (Chile) under the program 080.D-0368(A).

(2005) who found that the formation of young stellar populations in the LMC bar is associated with efficient SF in the last few Gyr (in particular, ~ 2 Gyr ago). A comprehensive spectroscopic study of field populations was performed by Cole et al. (2005) measuring the infrared CaII triplet of 373 giant stars located around the center of the bar. They found a distribution peaked at $[\text{Fe}/\text{H}] \sim -0.4$ dex with a low metallicity tail reaching $[\text{Fe}/\text{H}] \lesssim -2.0$ dex. Carrera et al. (2008) have measured the infrared CaII triplet in four fields at different radial distances ($\sim 3^\circ$, 5° , 6° and 8° , that is between 2.6 and 7 kpc) from the center of LMC. They found an average $[\text{Fe}/\text{H}] \sim -0.5$ dex for the closest fields, a lower $[\text{Fe}/\text{H}] \sim -0.8$ dex was found only in the more distant one. A detailed spectroscopic analysis of 59 giant stars located in the inner disk at ~ 1.2 kpc from the center was performed by Pompéia et al. (2008), who found a distribution peaked at $[\text{Fe}/\text{H}] \sim -0.75$ dex.

This paper is part of a project devoted to investigate the kinematic and chemical properties of the stellar populations in the LMC through the use of high-resolution spectra, able to provide accurate information about the kinematics, the metallicity and the chemical abundance of individual elements of these stars. Previous papers of the project have discussed the properties of old (Mucciarelli et al. 2009, 2010), intermediate-age (Ferraro et al. 2006; Mucciarelli et al. 2008) and young (Mucciarelli et al. 2011, 2012) globular clusters (GC) in the LMC. This paper is the first of the project dedicated to the kinematic and chemical characterization of the LMC field stellar populations: we present chemical patterns for a sample of 89 Red Giant Branch (RGB) stars members of the LMC and located in the field around the old metal-poor GC NGC 1786. This represents to date the largest sample of field giants in the LMC for which high-resolution spectra have been obtained.

2. Observations

We have observed 91 stars located in the region surrounding the old GC NGC 1786 at $\sim 2^\circ$ NW from the center of the LMC (Kim et al. 1998). The spectra have been acquired with the multi-object spectrograph FLAMES (Pasquini et al. 2002) at the Kueyen ESO-VLT telescope.

The spectroscopic targets have been selected by using the near-infrared (J, H and K bands) photometric catalog, obtained by combining the SOFI catalog for the inner ~ 2.5 arcmin, corresponding to the area covered by the GC NGC 1786 (see Mucciarelli et al. 2010 for details) and the Two Micro All Sky Survey (2MASS) catalog for the outermost region, in order to sample the surrounding field population. The final catalog was placed onto the 2MASS photometric and absolute astrometric system by following the standard procedure used in Ferraro et al. (2004). Photometric uncertainties are of about 0.01-0.02 and 0.03-0.05

for SOFI and 2MASS target, respectively. The targets have been selected along the RGB and in the magnitude range $K_0 \sim 12.3$ –14.0, in order to reach a sufficient SNR (> 30 –40) and excluding stars brighter than the magnitude level ($K_0 \sim 12.3$, see Cioni et al. 2006) of the RGB Tip of the intermediate-age LMC population.

Observations consists of a series of 45-minute-long exposures obtained with HR11 (5600–5840 Å and $R = 24200$) and HR13 (6120–6400 Å and $R = 22500$) gratings by using the GIRAFFE/MEDUSA configurations. The data reduction was performed with the GIRAFFE ESO pipeline that includes bias subtraction, flat fielding, wavelength calibration and spectrum extraction. Individual stellar spectra have been cleaned from the sky contribution, by subtracting the corresponding median sky spectrum. Finally, multiple spectra of each target have been coadded, reaching a SNR per pixel of ~ 40 in the faintest stars and up to ~ 100 in the brightest ones. Identification number, right ascension and declination of each target are listed in Table 1.

3. Kinematic and chemical analysis

Radial velocities (v_r) have been measured by means of the DAOSPEC code (Stetson & Pancino 2008). For each star, the spectra from the two different gratings have been analysed independently and the derived v_r averaged together by using the individual uncertainty as weight. Typical internal errors (computed as $\sigma/\sqrt{N_{lines}}$) are ~ 0.15 –0.20 km s⁻¹. Finally, we applied the heliocentric correction to each v_r .

The chemical analysis has been performed by using the suite of codes developed by R.L.Kurucz (see Sbordone et al. 2004) aimed to computing abundances from the observed equivalent widths (EWs) and synthetic spectra. The model atmospheres were computed with the ATLAS9 code, assuming plane-parallel geometry, local thermodynamical equilibrium for all species and without the inclusion of the approximate overshooting in the computation of the convective flux. The ATLAS9 model atmospheres were calculated with the new set of Opacity Distribution Functions by Castelli & Kurucz (2004).

The line list has been selected starting from the Kurucz/Castelli data² and updated with recent laboratory data from VALD and NIST databases. We included only transitions with theoretical/laboratory atomic data and checked against spectral blendings through the inspection of suitable synthetic spectra convolved at the GIRAFFE resolution. In particular, we adopted for the Fe lines the atomic data from the critical compilations by

²<http://wwwuser.oat.ts.astro.it/castelli/linelists.html>

Fuhr, Martin & Wiese (1988) and Fuhr & Wiese (2006), that represent the most updated dataset of theoretical/laboratory log gf for the iron lines.

For some unblended transitions for which theoretical/laboratory oscillator strengths are not available (or for those lines not well reproduced in the solar spectrum) we derived astrophysical oscillator strengths (labelled as SUN in Table 2) by using the solar flux spectra of Neckel & Labs (1984) and the model atmosphere for the Sun computed by F. Castelli³ adopting the solar abundances of Grevesse & Sauval (1998). We estimated for these oscillator strengths an accuracy < 15%, according to the uncertainties in the line profile fitting and in the continuum placement. We decide to include in our final linelist some Fe I transitions listed by Fuhr, Martin & Wiese (1988) and Fuhr & Wiese (2006) with high quoted uncertainties after the verification that these lines are well reproduced in the solar spectrum of Neckel & Labs (1984) and providing an iron abundance within ± 0.1 dex from the value of Grevesse & Sauval (1998).

Concerning the van der Waals damping constants, we adopted, whenever possible, the damping values by Barklem, Piskunov & O’Mara (2000), while for the other transitions the van der Waals constants were calculated according to Castelli (2005). The complete line list used is available in Table 2, including wavelength, element code, oscillator strength (and corresponding accuracy), lower excitational potential and reference source.

The atmospheric parameters have been derived as follows:

(1) A preliminary estimate of T_{eff} for each star was obtained from photometric $(J - H)_0$ and $(J - K)_0$ colors adopting an average color excess of $E(B - V) = 0.12$ (Persson et al. 1983), the extinction law by Rieke & Lebofsky (1985) and the color-temperature calibrations by Alonso et al. (1999) based on the Infra-Red Flux Method. The 2MASS magnitudes of our targets have been converted in the TCS photometric system (where the Alonso et al. (1999) relations are defined) by using the transformations provided by Carpenter (2001). We used the photometric T_{eff} as *first-guess values* and then we refined them by imposing the lack of any trend between Fe I abundances and the excitation potential χ . Basically, we find a good agreement between the photometric and spectroscopic T_{eff} , with an average difference of $T_{\text{eff}}^{\text{spec}} - T_{\text{eff}}^{\text{phot}} = 139$ K ($\sigma = 173$ K). Finally, the spectroscopic T_{eff} have been adopted for the following analysis. Typical uncertainties in the spectroscopic temperatures (calculated according to the slope in the plane A(Fe I) vs χ) ranging from ~ 80 up to ~ 130 K.

(2) Microturbulent velocities have been derived by requiring the lack of any trend between Fe I abundances and the reduced EW (defined as $\lg(EW/\lambda)$). Typical uncertainty in

³<http://wwwuser.oat.ts.astro.it/castelli/sun/ap00t5777g44377k1odfnew.dat>

the v_t determination is 0.1-0.2 km/s.

(3) Surface gravities have been estimated from the photometry, because the classical method to infer $\log g$ from the comparison between Fe I and Fe II lines cannot be applied, due to the small number of available Fe II lines in our spectra. Surface gravities have been derived from the Stefan-Boltzmann relation, using for each target the corresponding spectroscopic T_{eff} . We adopted the distance modulus $(m - M)_0 = 18.50$ (Alves 2004) and a typical evolutionary mass ($1.5 M_{\odot}$) for all the targets derived from a BaSTI (Pietrinferni et al. 2004) isochrone with age of 2 Gyr, $Z = 0.008$ and solar-scaled chemical mixture, according to the values estimated for the bulk of the LMC disk population by Bekki & Chiba (2005) and Cole et al. (2005). The luminosities are derived from the M_K -band magnitude using the bolometric corrections of Buzzoni et al. (2010). Internal errors in the derived $\log g$ (calculated by taking into account the uncertainties in the spectroscopic T_{eff} , mass and luminosity) are of about 0.1-0.15 dex. The photometric estimates of temperatures and gravities together with those obtained from spectroscopy are listed in Table 3.

EWs were measured with DAOSPEC. The abundances of Fe and Si have been obtained from the EWs. O abundances have been derived from the forbidden line at 6300.31 \AA by employing spectral synthesis technique. The abundances have been determined from χ^2 -minimization between the observed spectrum and a grid of synthetic spectra computed with the corresponding atmospheric parameters and convolved at the GIRAFFE resolution. Mg abundances have been derived with the same technique by using the strong line 5711.09 \AA ; we decide to exclude the Mg triplet at $\sim 6318 \text{ \AA}$ because these weak lines are located on the red wing of a close auto-ionization Ca line. This produce a decrease of the continuum level which was not easily measurable with DAOSPEC. The final abundances are expressed in the usual spectroscopic formalism (logarithmic scale in unit of solar abundances) and adopting the solar values from Grevesse & Sauval (1998) except for oxygen, for which we used the value by Caffau et al. (2010). All the abundance ratios of our sample are listed in Table 4.

4. Abundance uncertainties

For each abundance ratio we take into account two source of uncertainties, the internal error relative to the EW measurements and that arising from the uncertainties in the atmospheric parameters.

Uncertainties for each abundance ratio due to the uncertainties in the EW measurements have been estimated (for each star) by dividing the line-to-line scatter by the square root of the number of used lines. DAOSPEC provides also for each measured spectral line an

error computed from the standard deviation of the local flux residuals (representing a 68% confidence interval on the derived value of the EW). These uncertainties have been used only in the computation of the slopes in the A(Fe I) vs χ and A(Fe I) vs EWR planes (see Section 3).

Recently, Venn et al. (2012) pointed out that the internal EW errors provided by DAOSPEC are under-estimated of a factor of 2 with respect to those derived with the classical formula by Cayrel (1988), probably due to the pixel correlation during the wavelength calibration. We checked this effect in our data, assuming the FWHM estimated by DAOSPEC and the proper SNR for each spectrum. On average, we found a general agreement between the two sets of uncertainties (within $\pm 10\text{-}20\%$) but not a systematic effect. However, the DAOSPEC errors provide an internal ranking among the measured lines in a given star and possible systematic under/over-estimates do not afflict our results.

For O and Mg, for which we derived the abundances from spectral synthesis of only one line each, the uncertainty in the measurement has been estimated by resorting to Monte Carlo simulations. We study some stars as representative of the different SNR of our targets. We injected Poisson noise into the best-fit synthetic spectrum according to the SNR of the observed spectrum and we repeated the fit procedure; for each line we performed a total of 500 Monte Carlo events, assuming as uncertainty in the fitting procedure 1σ of the abundances distribution. For the O line (falling in the HR13 grating), the derived uncertainties are of 0.04, 0.03 and 0.02 dex at SNR= 30, 50 and 80 respectively, while for the Mg line (falling in the HR11 grating) we obtained uncertainties of 0.13, 0.09 and 0.04 dex for SNR= 30, 40 and 70.

We estimated also the uncertainty due to the continuum location, by using the root mean square of the residual provided by DAOSPEC, after removing all the fitted lines from the observed spectrum. For our stars the typical dispersion of the residual spectra is of $\pm 3\text{-}4\%$, corresponding to an error in the abundances less than 0.1 dex. Keeping in mind that DAOSPEC estimates a global continuum along the entire spectrum (and not a local continuum for each individual transition), this uncertainty can be considered as a systematic errorbar for all the lines in a given spectrum.

The uncertainty arising from the atmospheric parameters has been computed following the approach described by Cayrel et al. (2004). The usual method to derive the errors due to the stellar parameters is to vary one only parameter each time, keeping the other ones fixed and finally adding in quadrature the derived abundance variations. Obviously, this method does not take into account the correlations among the atmospheric parameters, providing only a conservative value for the uncertainty. In our case, T_{eff} and v_t have been optimized spectroscopically (and $\log g$ has been derived according to the spectroscopic temperature),

thus all the parameters are not independent each other. For each star, the temperature has been varied by $\pm 1\sigma_{T_{\text{eff}}}$, because the uncertainty in T_{eff} dominates the derived abundances as pointed out by Cayrel et al. (2004). Then, we repeated the optimization procedure described above by keeping the temperature fixed and deriving new values for $\log g$ and v_t . The advantage of this method is to naturally take into account the covariance terms among the parameters (see also Shetrone et al. 2003). The procedure has been repeated independently for each star by considering the corresponding T_{eff} uncertainty computed from the error of the slope in the $A(\text{Fe})-\chi$ plane. Table 5 lists the results of this procedure for a representative star of our sample: the second column shows the final uncertainty for each abundance ratio, while the other columns are the results obtained with the usual approach to vary independently each parameter. Last column of Table 5 is the sum in quadrature of the uncertainties due to one only parameter: these values are larger than those obtained with the Cayrel et al. (2004) approach because the covariances among the parameters is neglected. Typical abundance uncertainties due to the atmospheric parameters are of the order of $[\text{Fe}/\text{H}] = \pm 0.03$ dex, $[\text{O}/\text{Fe}] = \pm 0.04$ dex, $[\text{Mg}/\text{Fe}] = \pm 0.06$ dex and $[\text{Si}/\text{Fe}] = \pm 0.09$ dex.

Finally, the total internal error for each abundance ratio was obtained by adding in quadrature the error associated to EW measurements and atmospheric parameters. For $[\text{Fe}/\text{H}]$ it turns out to be of the order of $\sim 0.04\text{-}0.05$ dex because of the large number of measured lines.

5. Results

The heliocentric radial velocity distribution of the stars in our sample is shown in the left panel of Figure 1. Stars with radial velocity in the range $170 \leq v_r \leq 380 \text{ km s}^{-1}$ are considered LMC members, according to Zhao et al. (2003): only 2 stars with $v_r \sim 100 \text{ km s}^{-1}$ have been excluded (likely belonging to the Galaxy). The mean velocity of the sample is $v_r = 259.3 \text{ km s}^{-1}$ ($\sigma_v = 33.9 \text{ km s}^{-1}$), in good agreement with previous measurements in other samples of LMC disk by Cole et al. (2005), Carrera et al. (2008) and Pompéia et al. (2008).

The metallicity distribution of our sample is shown in the right panel of Figure 1. The entire sample has an average $[\text{Fe}/\text{H}] = -0.58$ dex ($\sigma_{[\text{Fe}/\text{H}]} = 0.25$ dex). Also, two main components can be distinguished:

1. A principal component (hereafter LMC-R) comprising $\sim 84\%$ of the observed sample with $[\text{Fe}/\text{H}] > -0.7$ dex, peaked at $[\text{Fe}/\text{H}] = -0.48$ dex and with a quite small dispersion ($\sigma_{[\text{Fe}/\text{H}]} = 0.13$ dex).

2. A secondary component (hereafter LMC-P), comprising $\sim 16\%$ of the sample, peaked at $[\text{Fe}/\text{H}] = -1.06$ dex ($\sigma_{[\text{Fe}/\text{H}]} = 0.18$ dex) with an extended tail up to $[\text{Fe}/\text{H}] \sim -1.5$ dex.

The peak of the metallicity distribution of LMC-R (see Fig. 2, a) is in good agreement with those obtained by Cole et al. (2005) ($[\text{Fe}/\text{H}] = -0.45$ dex, $\sigma_{[\text{Fe}/\text{H}]} = 0.31$ dex) (see Fig. 2, b) from the central bar and Carrera et al. (2008) ($[\text{Fe}/\text{H}] = -0.47$ dex ($\sigma_{[\text{Fe}/\text{H}]} = 0.30$ dex), $[\text{Fe}/\text{H}] = -0.50$ dex ($\sigma_{[\text{Fe}/\text{H}]} = 0.44$ dex) and $[\text{Fe}/\text{H}] = -0.45$ dex ($\sigma_{[\text{Fe}/\text{H}]} = 0.31$ dex) for the fields located at $\sim 3^\circ$, 5° and 6° at north of LMC center, respectively). A distribution peaked at a slightly lower value ($[\text{Fe}/\text{H}] = -0.75$ dex, $\sigma_{[\text{Fe}/\text{H}]} = 0.23$ dex) was found by Pompéia et al. (2008) (see Fig. 2).

Figure 3 shows the behaviour of O, Mg and Si, as a function of $[\text{Fe}/\text{H}]$. We plotted for comparison the abundance ratios measured in other environments: the Galaxy (including data for thin disk, thick disk and halo, by Venn et al. 2004; Reddy et al. 2006), the LMC disk (Pompéia et al. 2008), the nearby dwarf spheroidals (Shetrone et al. 2001, 2003; Letarte et al. 2010; Lemasle et al. 2012; Venn et al. 2012), the Sagittarius dwarf galaxy (Sbordone et al. 2007) and the old and intermediate-age LMC GCs (Johnson et al. 2006; Mucciarelli et al. 2008, 2009, 2010)⁴.

The $[\text{O}/\text{Fe}]$ ratio appears systematically lower than those measured in the Galaxy and basically consistent with those by Pompéia et al. (2008), even if they provide a few of measures for this abundance ratio. The $[\text{Mg}/\text{Fe}]$ ratio turns out to be subsolar in the entire metallicity range and ever lower than the Milky Way stars; also, our targets show lower Mg abundances with respect to those measured by Pompéia et al. (2008) and we attribute such a discrepancy to the different values of oscillator strengths and damping constants for the Mg line at 5711 \AA employing in the two analysis. Finally, the $[\text{Si}/\text{Fe}]$ ratio seems to be barely consistent with the Galactic stars, despite a larger dispersion.

Figure 4 shows the behaviour of the average $[\alpha/\text{Fe}]$ ratio, obtained by averaging the abundances of O, Mg and Si, as a function of $[\text{Fe}/\text{H}]$. We compared our targets with the $[\alpha/\text{Fe}]$ ratios of the other samples calculated by averaging the available α -element abundance ratios; only for the old LMC GCs we excluded O and Mg, because of the intrinsic star-to-star variations of these elements due to the self-enrichment process occurred in the early stages of these clusters (at variance to the intermediate-age LMC GCs where intrinsic spread in

⁴We excluded from this comparison the LMC GCs younger than 0.5 Gyr by Mucciarelli et al. (2011, 2012) because they are associated to the last episodes of star formation, while all the targets discussed here belong to the RGB, thus they are older than $\sim 1\text{-}2$ Gyr.

O and Mg content are not detected). The overall trend of the $[\alpha/\text{Fe}]$ ratio with the $[\text{Fe}/\text{H}]$ abundance shows a decrease at increasing metallicity. The most metal-poor stars with $[\text{Fe}/\text{H}] < -0.7$ dex show an $[\alpha/\text{Fe}]$ ratios larger than solar value, while stars with $[\text{Fe}/\text{H}] > -0.7$ dex show $[\alpha/\text{Fe}]$ ratio from solar to sub-solar values. For a given $[\text{Fe}/\text{H}]$, the $[\alpha/\text{Fe}]$ ratio measured in the LMC appears systematically lower than those measured in the Galaxy.

A substantial agreement of our abundances was generally found with the values measured in dSphs, in particular with the abundance ratios observed in the metal-poor component of the Sagittarius dwarf galaxy (Sbordone et al. 2007): such a similarity of α -elements, metallicity distribution and fraction of metal-poor stars has been already suggested by Monaco et al. (2005).

6. Discussion and Conclusions

We determined kinematic and chemical properties for 89 giant stars members of the disk of the LMC. This sample increases significantly the number of stars analysed so far through high-resolution spectroscopy (the largest sample observed by Pompéia et al. 2008 includes 59 stars).

The derived metallicity distribution is dominated by LMC-R, a metal-rich and narrow component peaked at $[\text{Fe}/\text{H}] = -0.48$ dex, with a secondary component LMC-P peaked at $[\text{Fe}/\text{H}] = \sim -1.0$ dex and reaching $[\text{Fe}/\text{H}] = \sim -1.5$ dex (right panel of Fig. 1). As shown in Figure 5, the two components show similar kinematic properties, with similar average $\langle v_r \rangle$ (265.9 km s⁻¹ for LMC-R and 261 km s⁻¹ for LMC-P) and with a small increase of the velocity dispersion decreasing the metallicity ($\sigma_v = 25$ km s⁻¹ and $\sigma_v = 29.7$ km s⁻¹, respectively).

The kinematic and abundance distributions can be now compared to those observed in the stellar population of the GC NGC 1786. All the stars of our sample belong to the RGB, hence their age can range from ~ 1 -2 Gyr up to ~ 12 -13 Gyr, thus excluding very recent (last 500 Myr) burst of star formation. At variance to the stars belonging to a stellar cluster, the determination of the age for field stars through isochrone fitting is a dangerous and uncertain technique, because the position of a RGB star in the Color-Magnitude Diagram is weakly sensitive to the age and highly affected by uncertainties in the color excess, evolutive mass and distance. Even if precise ages for each target star cannot be determined, we can draw the timeline of the chemical evolution in this region of the LMC, by comparing our results with the recent simulations by Bekki & Chiba (2005) and the SFH inferred by Smecker-Hane et al. (2002), Harris & Zaritsky (2009) and Rubele et al. (2012) in different

regions of the LMC; unfortunately, there are no determinations of SFH in the region of our targets.

(1) NGC 1786 is an old LMC GC generated during the first burst of SF occurred ~ 12 – 13 Gyr ago. Following Bekki & Chiba (2005) a loose stellar halo of old stars with a velocity dispersion of about ~ 40 km s $^{-1}$ and a broad metallicity distribution is also expected to be formed during that event.

It is interesting to check whether some of the stars observed in our sample could belong to NGC 1786 or to the LMC halo. Note that Mucciarelli et al. (2009, 2010) found for NGC 1786 $\langle v_r \rangle = 264.3$ km s $^{-1}$ ($\sigma_v = 5.7$ km s $^{-1}$), $[\text{Fe}/\text{H}] = -1.75$ dex and $[\alpha/\text{Fe}] = 0.37$ dex. Figure 5 shows that none of the observed stars has kinematic and chemical properties compatible with the population of NGC 1786. In particular, the observed sample has a systematically higher $[\text{Fe}/\text{H}]$ ($\gtrsim -1.0$ dex) and a lower $[\alpha/\text{Fe}]$ ($\lesssim 0.20$ dex), thus demonstrating that even LMC-P did not originate in the cluster.

This evidence could be used to put some constraints on the presence of old metal-poor α -enhanced stars in the sampled LMC disk field, which turns out to be less than $\sim 1\%$. Our outcome provides a substantial confirmation of the results by Cole et al. (2005), who found $\sim 3\%$ of their sample with $[\text{Fe}/\text{H}] < -1.5$ dex (but no measurements of $[\alpha/\text{Fe}]$ ratio are available) and by Pompéia et al. (2008), who found $\sim 2\%$, although the abundance patterns are incompatible with old LMC GCs. Since these samples cover different regions of the galaxy, the measured similar fraction of metal-poor stars in these three samples seems to suggest that the old, metal-poor component is distributed in a quite homogeneous way along the LMC disk.

(2) After the initial burst, the LMC has undergone a long period characterized by a continuous SF with low efficiency. The occurrence of this quiescent period in the LMC field is clearly visible in the SFH provided by Smecker-Hane et al. (2002), Harris & Zaritsky (2009) and Rubele et al. (2012), where a prolonged phase with very low or lacking SF is appreciable between ~ 4 – 5 Gyr and ~ 12 Gyr ago. This quiescent period is predicted also by the theoretical models proposed by Bekki & Chiba (2005) that derived a typical SF efficiency in this age range of ~ 0.1 M $_{\odot}$ yr $^{-1}$.

During this period, the LMC evolved in isolation, without gravitational interactions with the Galaxy and the SMC (Bekki & Chiba 2005; Besla et al. 2007). LMC-P likely formed during this period, as also suggested by the lower (by ~ 0.2 – 0.3 dex) $[\alpha/\text{Fe}]$ ratio with respect to the Galactic values at similar metallicity, which indicate that during this long period mainly SNeIa contribute to the gas enrichment.

If this scenario is correct, these stars were born during the period in which no GC formed

(the so-called *Age Gap*, Rich et al. 2001; Bekki et al. 2004), hence they are unique tracers of the LMC chemical evolution history between ~ 12 and 3 Gyr ago.

We also notice that the LMC-P fraction ($\sim 16\%$) is larger than that ($\lesssim 10\%$) found by Cole et al. (2005). This is probably due to different location of the two fields. The sample analysed by Cole et al. (2005) is located around the central bar (at variance with our targets, located in the inner disk at ~ 1.8 kpc from the LMC center). Infact, Bekki & Chiba (2005) suggest that the central bar formed in the last 3–4 Gyr with a marginal fraction of metal-poor stars in its stellar content.

Also, it is interesting to notice that the $[\alpha/\text{Fe}]$ ratio of this stellar component well resembles the mean locus defined by the dSph stars (grey triangles in the lower panel of Fig. 4, but see also Fig.11 in Tolstoy, Hill & Tosi (2009)), suggesting similar chemical enrichment histories.

(3) LMC-R formed during the relevant burst of SF occurred in the last few Gyr probably due to the tidal capture of the SMC by the LMC. Numerical simulations (Bekki & Chiba 2005) predict that first close encounter between the two Clouds occurred ~ 3 –4 Gyr ago, when the LMC and SMC become a gravitational bound system. This strong interaction triggered the SFR up to $\sim 0.4 M_{\odot} \text{ yr}^{-1}$. The occurrence of this SF enhancement has been confirmed by Harris & Zaritsky (2009) by using Color-Magnitude Diagrams of different regions of the LMC. However, the binary system status of Magellanic Clouds and its timescales is still a matter of debate since there is no unambiguous consensus between dynamical simulation and photometric studies. For instance, Rubele et al. (2012) analysed new photometric dataset from the Vista Magellanic Survey, finding an enhancement of star formation with a peak at ~ 2 Gyr and in some regions a second peak at ~ 5 Gyr and interpreted as the epoch of tidal interaction between the LMC and the Galaxy. Conversely, Besla et al. (2007) suggested that the LMC-SMC system is on its first close passage about the Galaxy, being entered in the Milky Way virial radius only in the last 1-3 Gyr.

LMC-R distribution is very narrow ($\sigma_{[\text{Fe}/\text{H}]} = 0.13$ dex), suggesting that the episode of SF associated to the first close encounter between the two Clouds has been very efficient (in order to produce the majority of the LMC disk stars) and fast, because the stars have not had time to furtherly enrich in iron. These stars show $[\alpha/\text{Fe}]$ abundance ratios that are close to the solar value, in nice agreement with the values measured in the intermediate-age GCs (Mucciarelli et al. 2008) with age of 1–3 Gyr, as shown in Figure 4.

The observed $[\alpha/\text{Fe}]$ ratios agree with those derived in the Sagittarius dSph giants (asterisks in lower panel of Fig. 4), while the nearby dSphs studied so far do not reach such metallicity. The most metal-rich stars discussed by Letarte et al. (2010) in Fornax show

$[\text{Fe}/\text{H}] \sim -0.6$ dex, consistent with the metal-poor edge of the LMC-R population. These evidences (the similarity with Sgr and the difference with the nearby dSphs) seem to confirm that the recent SFH of the LMC has been quite complex and turbulent, and the stars of the LMC-R population (that dominates the metallicity distribution of our sample) are the products of the tidal interactions occurring among LMC, SMC and our Galaxy.

The intrinsic dispersion of each individual abundance ratio of the LMC-R population suggests a high degree of homogeneity, pointing out that an efficient and homogeneous mixing of the SN ejecta occurs. We note that the dispersion of the $[\alpha/\text{Fe}]$ ratios in these stars is larger than the range of values covered by the intermediate-age GCs.

Thus, the scatter in $[\alpha/\text{Fe}]$ abundances of the LMC-R stars reflects the larger age range in which these stars formed. However, we find a general agree between the values observed in the field and GC stars in this metallicity range, suggesting in any case a common origin of these stars from similar burst of SF.

It is important to recall that there is an offset between the age of the onset of the SF in the LMC field and that of the GC formation. In fact, if the SF in the field started about 4-5 Gyr ago (the precise age depends on the location in the disk and the magnitude of the tidal interactions with the SMC), the GC formation restarts about 2 Gyr ago, as suggested also by Bekki & Chiba (2005). This difference is confirmed by the measured ages in the intermediate-ages GCs (see e.g. Rich et al. 2001; Mucciarelli et al. 2007a,b) and the lack of globulars in the age range between 2 and 5 Gyr. Furthermore, the lower metallicity edge of LMC-R stars ($[\text{Fe}/\text{H}] \simeq -0.7$ dex), if compared to that of GCs, seems to support that the SF of field stars becomes efficient slightly before.

Recently, Tsujimoto & Bekki (2012) discussed the unusual low $[\text{Mg}/\text{Fe}]$ (-0.9 dex) ratio measured by Colucci et al. (2012) in the intermediate-age, metal-rich GC NGC 1718, suggesting that this cluster and a fraction of LMC field stars were formed from the metal-poor gas acquired by infall from the SMC about 1-2 Gyr ago (the so-called *Magellanic Squall*, Bekki & Chiba 2007). In our sample we did not detect metal-rich stars characterized by such low Mg or α -depletion, pointing out that the stars formed from metal-poor gas accreted by the SMC are (if any) a negligible ($<1\%$) fraction of the LMC disk.

The authors warmly thank the anonymous referee for his/her suggestions in improving the paper.

REFERENCES

- Alonso, A., Arribas, S., & Martínez-Roger, C. 1999, *A&AS*, 140, 261
- Alves, D. R. 2004, *NewAR*, 48, 659
- Barklem, P. S., Piskunov, N., & O’Mara, B. J., 2000, *A&AS*, 142, 467
- Bekki, K., Couch, W. J., Beasley, M. A., et al. 2004, *ApJ*, 610, L93
- Bekki, K., & Chiba, M. 2005, *MNRAS*, 356, 680
- Bekki, K., & Chiba, M. 2007, *MNRAS*, 381, L16
- Besla, G., Kallivayalil, N., Hernquist, L., et al. 2007, *ApJ*, 668, 949
- Brocato, E., Castellani, V., Ferraro, F. R., Piersimoni, A. M., & Testa, V. 1996, *MNRAS*, 282, 614
- Brocato, E., Castellani, V., Di Carlo, E., Raimondo, G., & Walker, A. R. 2003, *AJ*, 125, 3111
- Buzzoni, A., Patelli, L., Bellazzini, M., Pecci, F. F., & Oliva, E. 2010, *MNRAS*, 403, 1592
- Caffau, E., Ludwig, H.-G., Steffen, M., Freytag, B., & Bonifacio, P., 2011, *SoPh*, 268, 255
- Carrera, R., Gallart, C., Hardy, E., Aparicio, A., & Zinn, R. 2008, *AJ*, 135, 836
- Carpenter, J. M., 2001, *AJ*, 121, 2851
- Castelli, F., 2005, *MSAIS*, 8, 44
- Castelli, F., & Kurucz, R. L. 2004, [arXiv:astro-ph/0405087](https://arxiv.org/abs/astro-ph/0405087)
- Cayrel, R., 1988, in *IAU Symposium, Vol.132, The Impact of very high S/N spectroscopy on Stellar Physics*, ed. G. Cayrel de Strobel & M. Spite, 345
- Cayrel, R., et al., 2004, *A&A*, 416, 1117
- Cioni, M.-R. L., Girardi, L., Marigo, P., & Habing, H. J. 2006, *A&A*, 448, 77
- Cole, A. A., Tolstoy, E., Gallagher, J. S., III, & Smecker-Hane, T. A. 2005, *AJ*, 129, 1465
- Colucci, J. E., Bernstein, R. A., Cameron, S. A., & McWilliam, A. 2012, *ApJ*, 746, 29
- Ferraro, F. R., Origlia, L., Testa, V., & Maraston, C. 2004, *ApJ*, 608, 772

- Ferraro, F. R., Mucciarelli, A., Carretta, E. & Origlia, L., 2006, *ApJ*, 645L, 33
- Fuhr, J.R., Martin, G.A., & Wiese, W.L. 1988. *J.Phys.Chem.Ref.Data*, 17, 4.
- Fuhr, J.R., & Wiese, W.L., 2006, *J.Phys.Chem.Ref.Data*, 35, 1669
- Gallart, C., Zoccali, M., Bertelli, G., et al. 2003, *AJ*, 125, 742
- Garz, T., 1973, *A&A*, 26, 471
- Grevesse, N., & Sauval, A. J., 1998, *Space Science Reviews*, 85, 161
- Grocholski, A. J., Cole, A. A., Sarajedini, A., Geisler, D., & Smith, V. V. 2006, *AJ*, 132, 1630
- Johnson, J. A., Ivans, I. I., & Stetson, P. B. 2006, *ApJ*, 640, 801
- Harris, J., & Zaritsky, D. 2009, *AJ*, 138, 1243
- Kim, S., Staveley-Smith, L., Dopita, M. A., et al. 1998, *ApJ*, 503, 674
- Lemasle, B., Hill, V., Tolstoy, E., et al., 2012, *A&A*, 538, 100
- Letarte, B., Hill, V., Tolstoy, E., et al., 2010, *A&A*, 523, 17
- Monaco, L., Bellazzini, M., Bonifacio, P., Ferraro, F. R., Marconi, G., Pancino, E., Sbordone, L., & Zaggia, S., 2005, *A&A*, 441, 141
- Mucciarelli, A., Ferraro, F. R., Origlia, L., & Fusi Pecci, F., 2007, *AJ*, 133, 2053
- Mucciarelli, A., Origlia, L., & Ferraro, F. R., 2007, *AJ*, 134, 1813
- Mucciarelli, A., Carretta, E., Origlia, L., & Ferraro, F. R., 2008, *AJ*, 136, 375
- Mucciarelli, A., Origlia, L., Ferraro, F. R., & Pancino, E., 2009, *ApJ*, 659L, 134
- Mucciarelli, A., Origlia, L., & Ferraro, F. R. 2010, *ApJ*, 717, 277
- Mucciarelli, A., Cristallo, S., Brocato, E., et al. 2011, *MNRAS*, 413, 837
- Mucciarelli, A., Origlia, L., Ferraro, F. R., Bellazzini, M., & Lanzoni, B., 2012, *ApJ*, 746L, 19
- Neckel, H., & Labs, D., 1984, *SoPh*, 90, 205
- Olsen, K. A. G., Hodge, P. W., Mateo, M., et al. 1998, *MNRAS*, 300, 665

- Olszewski, E. W., Schommer, R. A., Suntzeff, N. B., & Harris, H. C. 1991, *AJ*, 101, 515
- Pasquini, L., Avila, G., Blecha, A., et al. 2002, *The Messenger*, 110, 1
- Persson, S. E., Aaronson, M., Cohen, J. G., Frogel, J. A., & Matthews, K. 1983, *ApJ*, 266, 105
- Pietrinferni, A., Cassisi, S., Salaris, M., & Castelli, F. 2004, *ApJ*, 612, 168
- Pompéia, L., Hill, V., Spite, M., et al. 2008, *A&A*, 480, 379
- Reddy, B. E., Lambert, D. L., & Allende Prieto, C. 2006, *MNRAS*, 367, 1329
- Rich, R. M., Shara, M. M., & Zurek, D. 2001, *AJ*, 122, 842
- Rieke, G. H., & Lebofsky, M. J., 1985, *ApJ*, 288, 618
- Rubele, S. et al. 2012, *A&A*, 537, 106
- Sbordone, L., Bonifacio, P., Castelli, F., & Kurucz, R. L., 2004, *MmSaI*, 75, 396
- Sbordone, L., Bonifacio, P., Buonanno, R., et al. 2007, *A&A*, 465, 815
- Shetrone, M. D., Côté, P., & Sargent, W. L. W. 2001, *ApJ*, 548, 592
- Shetrone, M., Venn, K. A., Tolstoy, E., et al. 2003, *AJ*, 125, 684
- Smecker-Hane, T. A., Cole, A. A., Gallagher, J. S., III, & Stetson, P. B. 2002, *ApJ*, 566, 239
- Stetson, P. B., & Pancino, E., *PASP*, 120, 1332
- Storey, P. J., & Zeippen, C. J., 2000, *MNRAS*, 312, 813
- Tsujimoto, T., & Bekki, K. 2012, arXiv:1204.4213
- Tolstoy, E., Hill, V. & Tosi, M., 2009, *ARA&A*, 47, 371
- Venn, K. A., Irwin, M., Shetrone, M. D., et al. 2004, *AJ*, 128, 1177
- Venn, K. A., Shetrone, M. D., Irwin, M., J. et al., 2012, *ApJ*, 751, 102
- Zhao, H., Ibata, R. A., Lewis, G. F., & Irwin, M. J. 2003, *MNRAS*, 339, 701

Table 1. Identification number, right ascension, declination and J, H, K magnitudes. The entire table is available in the online version.

ID	R.A. (J2000)	Dec. (J2000)	J (mag)	H (mag)	K (mag)
353	74.8429031	-67.7529373	14.55	13.80	13.61
1415	74.7569885	-67.7277374	14.52	13.75	13.57
1593	74.7403107	-67.7479858	14.34	13.56	13.36
1954	74.6953583	-67.7596817	14.11	13.28	13.12
1980	74.6899948	-67.7497635	14.52	13.74	13.58
2353	74.7275314	-67.7423553	12.56	11.87	11.71
2363	74.7172394	-67.7453918	14.67	13.97	13.82
2376	74.7086487	-67.7528458	14.62	13.93	13.81
90012	74.2391357	-67.7102280	13.91	13.05	12.93
90119	74.5899658	-67.9048157	14.27	13.38	13.23

Table 2. Wavelength, element, oscillator strength, excitation potential and reference source of adopted line list.

λ (Å)	El.	log gf	accuracy	E.P. (eV)	Ref.
5586.756	FeI	-0.144	<10%	3.37	Fuhr & Wiese (2006)
5607.664	FeI	-2.270	<50%	4.15	Fuhr, Martin & Wiese (1988)
5611.356	FeI	-2.990	<50%	3.64	Fuhr, Martin & Wiese (1988)
5618.632	FeI	-1.276	<18%	4.21	Fuhr & Wiese (2006)
5619.225	FeI	-3.270	<50%	3.69	Fuhr, Martin & Wiese (1988)
5619.595	FeI	-1.670	>50%	4.39	Fuhr & Wiese (2006)
5624.022	FeI	-1.140	<15%	4.39	SUN
5633.946	FeI	-0.320	>50%	4.99	Fuhr & Wiese (2006)
5636.696	FeI	-2.560	>50%	3.64	Fuhr & Wiese (2006)
5638.262	FeI	-0.840	<50%	4.22	Fuhr & Wiese (2006)
5640.307	FeI	-1.700	<15%	4.64	SUN
5646.684	FeI	-2.500	<50%	4.26	Fuhr, Martin & Wiese (1988)
5650.690	FeI	-0.960	>50%	5.09	Fuhr & Wiese (2006)
5651.469	FeI	-2.000	<50%	4.47	Fuhr, Martin & Wiese (1988)
5652.318	FeI	-1.920	>50%	4.26	Fuhr & Wiese (2006)
5653.867	FeI	-1.610	>50%	4.39	Fuhr & Wiese (2006)
5661.021	FeI	-2.430	<50%	4.58	Fuhr, Martin & Wiese (1988)
5661.345	FeI	-1.756	<10%	4.28	Fuhr & Wiese (2006)
5662.516	FeI	-0.573	<10%	4.18	Fuhr & Wiese (2006)
5677.684	FeI	-2.700	<50%	4.10	Fuhr, Martin & Wiese (1988)
5678.601	FeI	-4.670	<50%	2.42	Fuhr, Martin & Wiese (1988)
5680.240	FeI	-2.540	>50%	4.19	Fuhr & Wiese (2006)
5691.497	FeI	-1.490	>50%	4.30	Fuhr & Wiese (2006)
5693.640	FeI	-0.680	<15%	4.96	SUN
5704.733	FeI	-1.250	<15%	5.03	SUN
5705.465	FeI	-1.355	<10%	4.30	Fuhr & Wiese (2006)
5714.551	FeI	-1.770	<15%	5.09	SUN
5720.886	FeI	-1.950	<50%	4.55	Fuhr, Martin & Wiese (1988)
5731.762	FeI	-1.270	<50%	4.26	Fuhr & Wiese (2006)
5732.296	FeI	-1.560	<25%	4.99	Fuhr, Martin & Wiese (1988)
5741.848	FeI	-1.670	<25%	4.26	Fuhr & Wiese (2006)
5760.345	FeI	-2.440	>50%	3.64	Fuhr & Wiese (2006)
5767.972	FeI	-3.200	<15%	4.29	SUN
5775.081	FeI	-1.298	<18%	4.22	Fuhr & Wiese (2006)
5776.224	FeI	-3.400	<15%	3.69	SUN
5778.453	FeI	-3.430	<25%	2.59	Fuhr & Wiese (2006)
5793.915	FeI	-1.660	>50%	4.22	Fuhr & Wiese (2006)

Table 2—Continued

λ (Å)	El.	log gf	accuracy	E.P. (eV)	Ref.
5805.757	FeI	-1.590	<25%	5.03	Fuhr, Martin & Wiese (1988)
5806.725	FeI	-1.030	<50%	4.61	Fuhr & Wiese (2006)
5811.915	FeI	-2.430	<50%	4.14	Fuhr, Martin & Wiese (1988)
6120.249	FeI	-5.970	<7%	0.91	Fuhr & Wiese (2006)
6151.618	FeI	-3.299	<10%	2.18	Fuhr & Wiese (2006)
6165.360	FeI	-1.474	<18%	4.14	Fuhr & Wiese (2006)
6187.989	FeI	-1.670	>50%	3.94	Fuhr & Wiese (2006)
6200.313	FeI	-2.437	<18%	2.61	Fuhr & Wiese (2006)
6226.734	FeI	-2.220	<50%	3.88	Fuhr, Martin & Wiese (1988)
6246.319	FeI	-0.877	<10%	3.60	Fuhr & Wiese (2006)
6252.555	FeI	-1.687	<10%	2.40	Fuhr & Wiese (2006)
6322.686	FeI	-2.426	<18%	2.59	Fuhr & Wiese (2006)
6330.849	FeI	-1.190	<15%	4.73	SUN
6335.330	FeI	-2.177	<18%	2.20	Fuhr & Wiese (2006)
6336.824	FeI	-0.856	<10%	3.69	Fuhr & Wiese (2006)
6380.743	FeI	-1.376	<25%	4.19	Fuhr & Wiese (2006)
6300.304	OI	-9.717	<2%	0.00	Storey & Zeippen (2000)
5711.095	MgI	-1.724	<10%	4.35	NIST
5665.555	SiI	-2.040	20%	4.92	Garz (1973)
5666.677	SiI	-1.710	<15%	5.62	SUN
5690.425	SiI	-1.870	20%	4.93	Garz (1973)
5701.104	SiI	-2.050	20%	4.93	Garz (1973)
5793.073	SiI	-2.060	20%	4.93	Garz (1973)
6155.144	SiI	-0.870	<15%	5.62	SUN
6237.319	SiI	-1.100	<15%	5.61	SUN

Table 3. Identification number, photometric temperature and gravity, radial velocity and spectroscopic atmospheric parameters for the stars in our sample. The entire table is available in the online version.

ID	$T_{\text{eff}}^{\text{phot}}$ (K)	$\log g^{\text{phot}}$ (dex)	v_r (km s ⁻¹)	$T_{\text{eff}}^{\text{spec}}$ (K)	$\log g^{\text{spec}}$ (dex)	[A/H] (dex)	v_t^{spec} (km s ⁻¹)
353	4074	1.12	269.7	4150	1.10	-0.50	1.50
1415	4043	1.10	223.6	4200	1.10	-0.50	1.80
1593	3989	1.01	254.2	4150	1.10	-0.50	1.60
1954	3922	0.91	223.3	3850	0.90	0.00	1.50
1980	4018	1.10	272.3	4100	1.10	-0.50	1.60
2353	4255	0.39	299.4	4350	0.40	-0.50	1.80
2363	4227	1.23	265.1	4350	1.30	-0.50	1.70
2376	4308	1.24	230.8	4600	1.30	-1.00	2.10
90012	3906	0.83	243.5	4000	0.80	-1.00	2.00
90119	3795	0.93	251.1	4450	1.20	-0.50	2.10

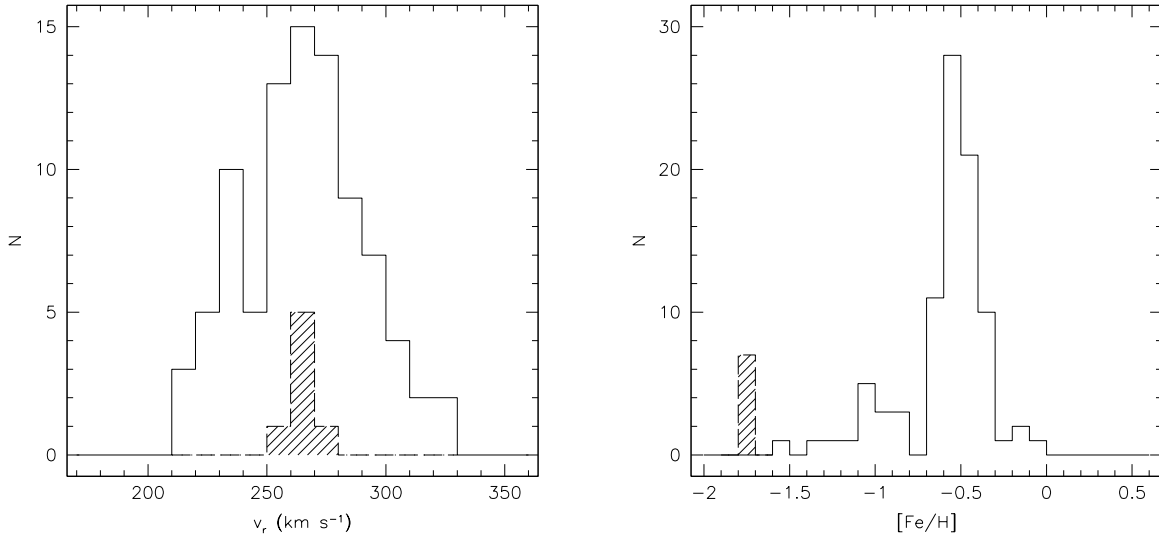


Fig. 1.— The heliocentric radial velocity distribution (left panel) and the metallicity distribution (right panel) of our sample of LMC disk stars. The shaded histograms show the distribution of the 7 member stars of NGC 1786 (Mucciarelli et al. 2009, 2010).

Table 4. Derived abundances for the stars of our sample. The entire table is available in the online version.

ID	[Fe/H] (dex)	[O/Fe] (dex)	[Mg/Fe] (dex)	[Si/Fe] (dex)
353	-0.42 ± 0.03	0.01 ± 0.05	-0.16 ± 0.08	-0.07 ± 0.06
1415	-0.62 ± 0.03	0.19 ± 0.04	-0.21 ± 0.02	0.16 ± 0.03
1593	-0.58 ± 0.02	0.04 ± 0.06	0.06 ± 0.09	0.14 ± 0.05
1954	-0.45 ± 0.03	-0.18 ± 0.09	-0.13 ± 0.10	0.17 ± 0.05
1980	-0.46 ± 0.02	0.06 ± 0.04	-0.22 ± 0.10	0.13 ± 0.02
2353	-0.37 ± 0.02	-0.38 ± 0.08	-0.16 ± 0.09	-0.09 ± 0.03
2363	-0.50 ± 0.03	-0.03 ± 0.07	-0.12 ± 0.10	0.03 ± 0.04
2376	-1.08 ± 0.03	0.28 ± 0.05	-0.14 ± 0.11	0.18 ± 0.06
90012	-1.24 ± 0.02	0.38 ± 0.09	0.02 ± 0.07	0.37 ± 0.07
90119	-0.64 ± 0.02	0.24 ± 0.09	-0.11 ± 0.13	-0.04 ± 0.05

Note. — The adopted solar values are 7.50, 8.76, 7.58 and 7.55 for Fe, O, Mg and Si.

Table 5. Abundance uncertainties for the star 91969. The second column is the total uncertainty estimated by following the prescriptions by Cayrel et al. (2004). The other columns show the variations in abundance due to the variation of one only parameter, while the last column is the sum in quadrature of these terms, without taking into account the covariance terms.

Element	Parameters uncertainty (dex)	δT_{eff} $\pm 100\text{K}$ (dex)	$\delta \log g$ ± 0.1 (dex)	δv_t $\pm 0.1 \text{ km s}^{-1}$ (dex)	Quadrature (dex)
Fe	± 0.01	± 0.03	± 0.02	± 0.04	± 0.05
O	± 0.02	± 0.01	± 0.05	± 0.02	± 0.05
Mg	± 0.04	± 0.03	± 0.01	± 0.02	± 0.04
Si	± 0.06	± 0.07	± 0.03	± 0.02	± 0.08

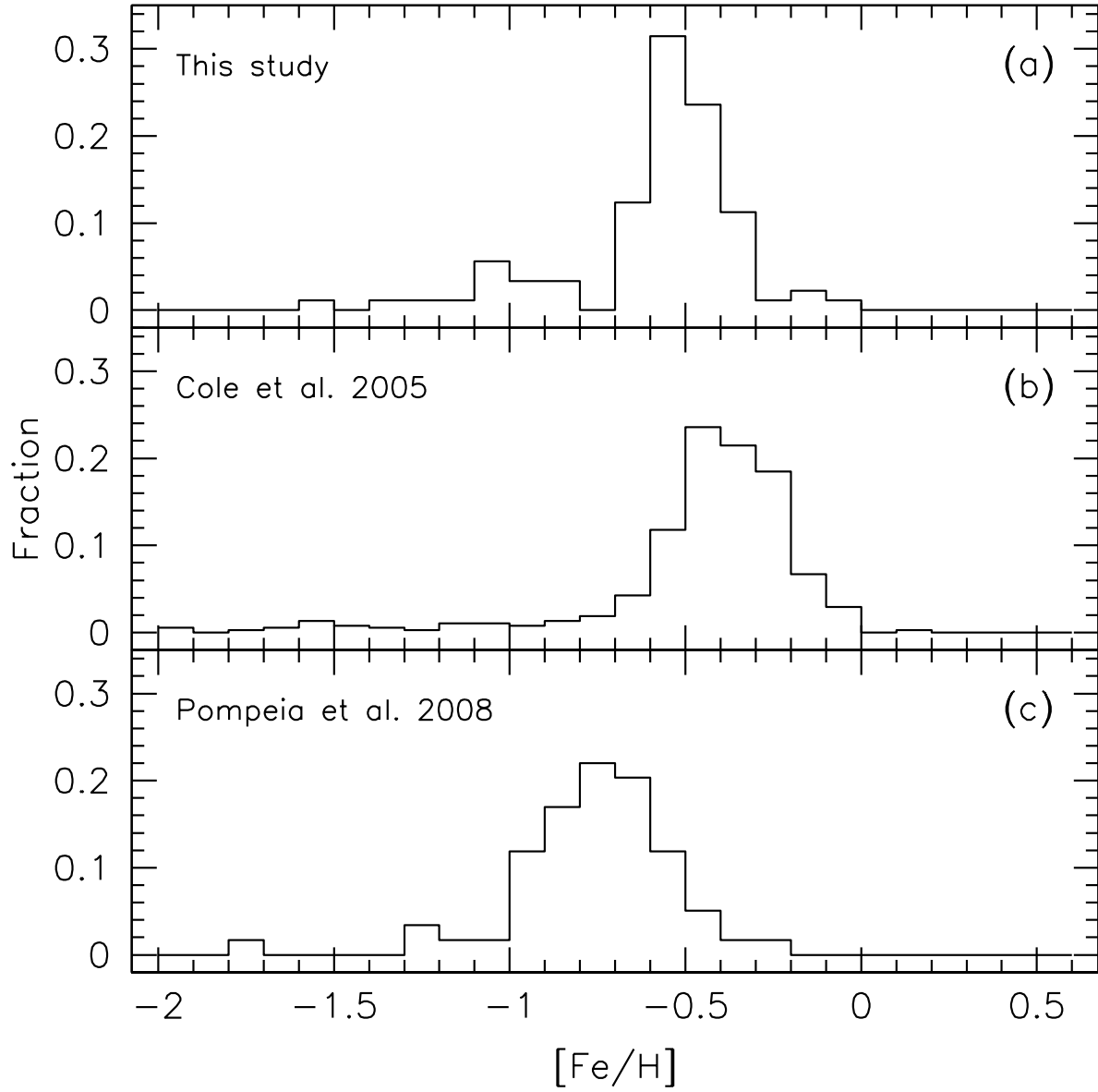


Fig. 2.— Comparison of our normalized metallicity distribution (a) with that one by Cole et al. (2005) (b) and Pompéia et al. (2008) (c).

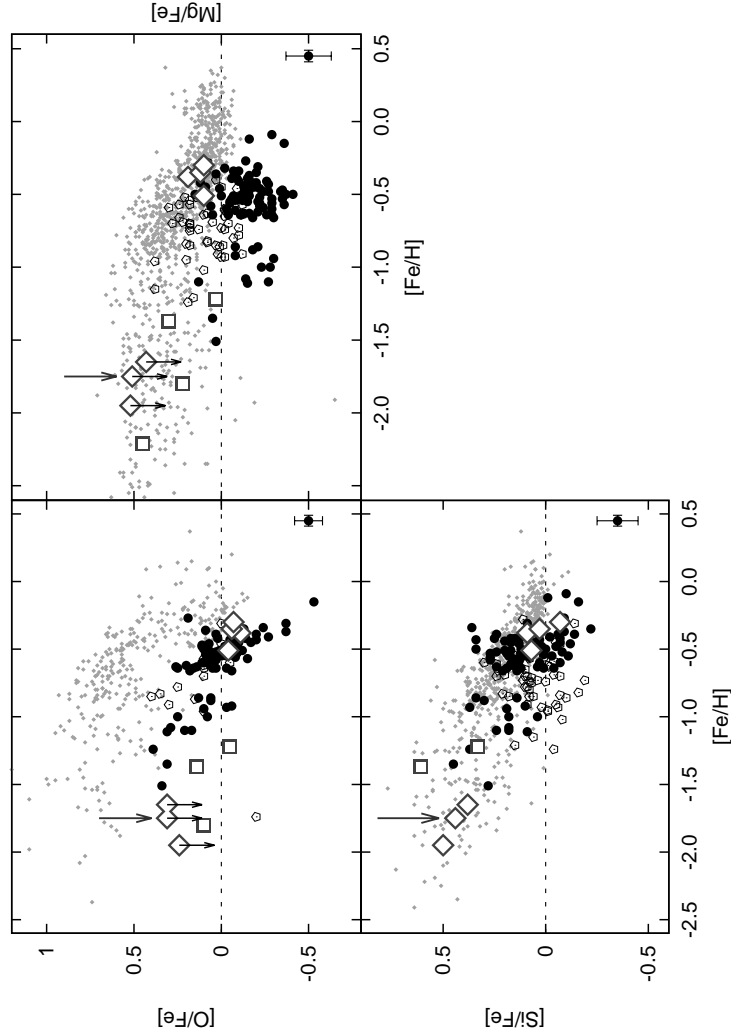


Fig. 3.— Behaviour of the $[O/Fe]$, $[Mg/Fe]$ and $[Si/Fe]$ ratio as a function of $[Fe/H]$. Black dots represent our targets, the small gray diamonds are the Galaxy data (Venn et al. 2004, Reddy et al. 2006), the black pentagons are the LMC disk (Pompéia et al. 2008), the edged white squares and diamonds are the old (Johnson et al. 2006; Mucciarelli et al. 2009, 2010) and intermediate-age LMC GCs (Mucciarelli et al. 2008), respectively. The $[Mg/Fe]$ abundance ratios from Pompéia et al. (2008) were corrected by a factor of $\simeq -0.11$ dex to take into account the effect of different oscillator strength for the line at 5711 \AA used in both analysis. The average $[O/Fe]$ and $[Mg/Fe]$ ratios of the three old and metal poor GCs from Mucciarelli et al. (2009) was obtained averaging the abundances of the stars with greater values only, in order to avoid the effects of anticorrelations. In this case the tiny black arrows indicate them as an “upper limit”. The dark-gray arrow marks the position of NGC 1786. Dashed lines mark the solar value. The error bars in the bottom right corner indicate the cumulative (EWs + atmospheric parameters) uncertainties.

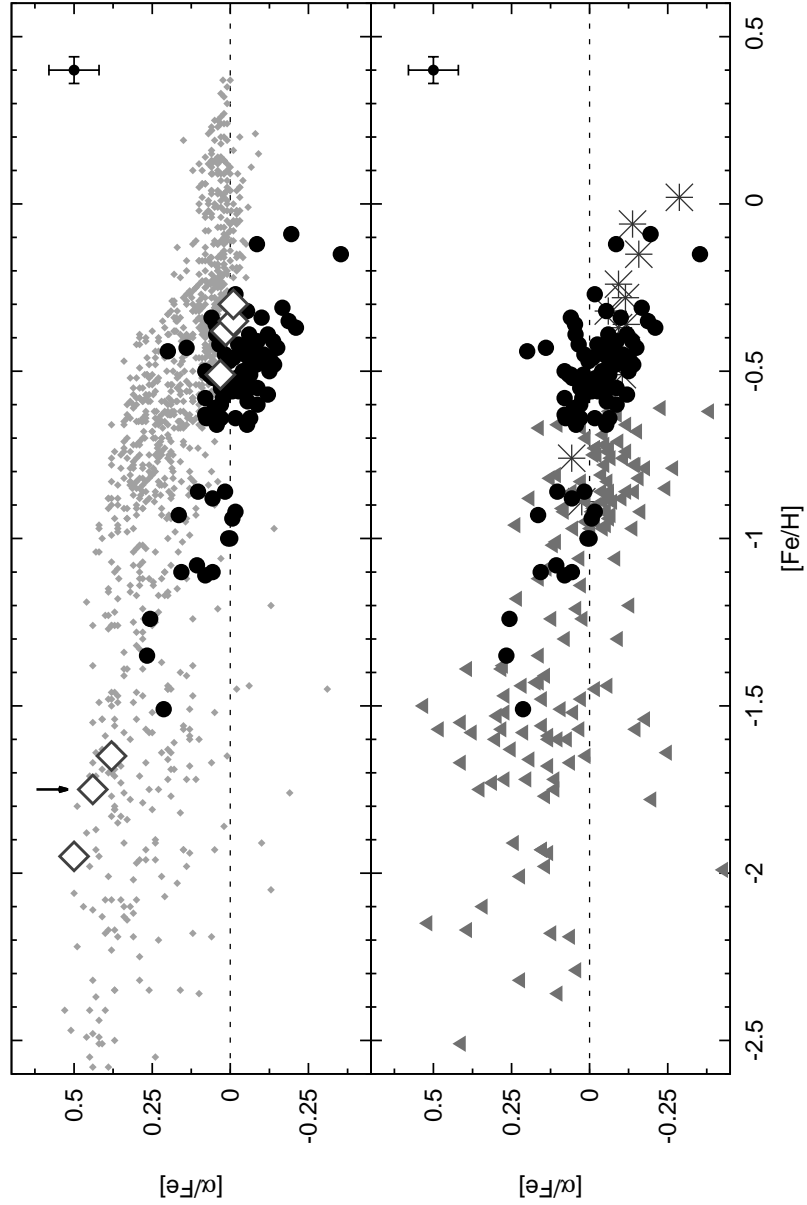


Fig. 4.— Behaviour of the average $[\alpha/\text{Fe}]$ ratio as a function of $[\text{Fe}/\text{H}]$. Same symbols of Figure 3. At variance with the intermediate-age GCs, the $[\alpha/\text{Fe}]$ ratio of the three old and metal poor GCs includes $[\text{Si}/\text{Fe}]$ only, in order to avoid the effect due to the intrinsic dispersion observed in the O and Mg abundances. Dashed lines mark the solar value. The error bars in the top right corner indicates the average uncertainty of iron and “ α -elements” abundances. Upper panel shows the comparison with the Galactic stars, while bottom panel shows the comparison with stars in the Sagittarius dwarf galaxy (asterisks) and in the nearby dwarf galaxies (grey triangles; the plotted samples include the data by Shetrone et al. (2001) and Shetrone et al. (2003) for Draco, Sextant, Ursa Minor, Sculptor, Fornax, Carina and Leo I, Letarte et al. (2010) for Fornax and Lemasle et al. (2012) and Venn et al. (2012) for Carina).

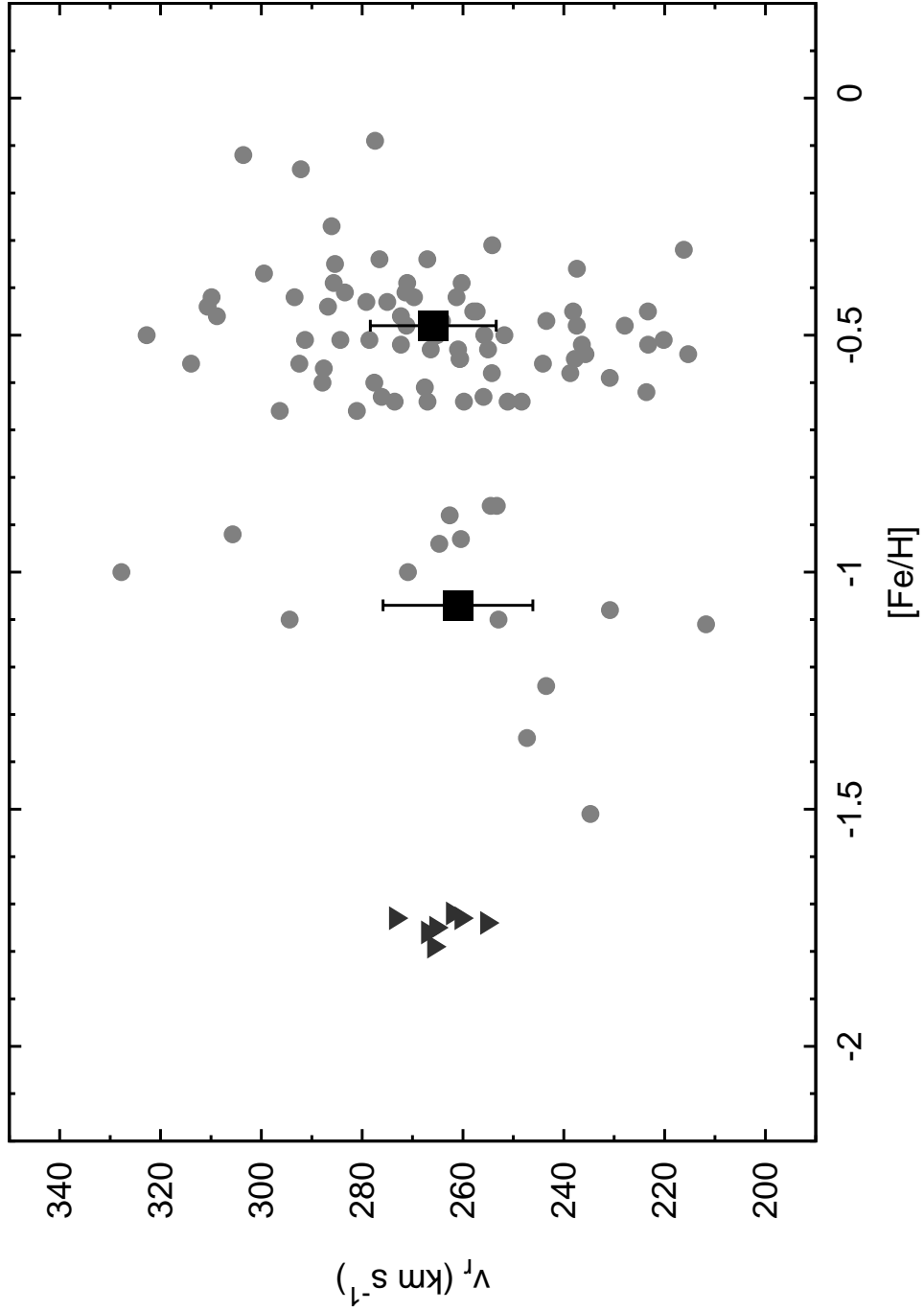


Fig. 5.— The distribution of our targets (gray points) in the $v_r - [\text{Fe}/\text{H}]$ plane with of the 7 member stars of NGC 1786 (black triangles) by Mucciarelli et al. (2009, 2010). The black squares represent the average radial velocities and metallicities of the two components.